A SIMPLE INDUCTION MACHINE MODEL FOR PREDICTING LOW FREQUENCY DYNAMICS

Sina Chini Foroosh, Liwei Wang, and Juri Jatskevich

University of British Columbia, Vancouver, Canada

ABSTRACT

Conventional models of induction machine for steady-state and dynamic analysis use fixed value of the rotor resistance; whereas for representing the deep-rotor-bar effect a second rotor branch is typically required therefore increasing the model complexity and order. This paper proposes a simple but very effective modification of traditional model, wherein a single-branch rotor resistance is changed as a function of speed. The new model parameters are readily identified using standard experiments and tests. Experimental results and simulation studies demonstrate the improved accuracy and advantage of the proposed model in predicting the low-frequency transients. More importantly, the improvement is achieved without increasing the model order.

Index Terms— induction machine, transient model, deep-rotor-bar effect, low frequency dynamics.

1. INTRODUCTION

There have been a large number of models proposed in the literature for representing various phenomena in induction machines. The modeling approaches range from highly accurate finite-element based models, magnetic-equivalent circuit, and coupled electrical circuit models which require the least amount of computational resources and therefore are widely used [1].

This paper is focused on modeling squirrel cage induction machines using coupled electrical circuit approach [1]. To accurately model a deep-rotor-bar effect, the rotor can be represented as a high-order transfer function. A corresponding steady-state equivalent circuit is depicted in Fig. 1(a). Based on this approach, an advanced dynamic qd model accounting for saturation and arbitrary rotor network has been proposed in [2]. This model is capable of predicting both high- and low-frequency phenomena with excellent accuracy as observed in currents and developed torque. Such models may therefore be used to study machine-inverter interactions, switching transients, and torque harmonics.

978-1-4244-1643-1/08/$25 © 2008 IEEE

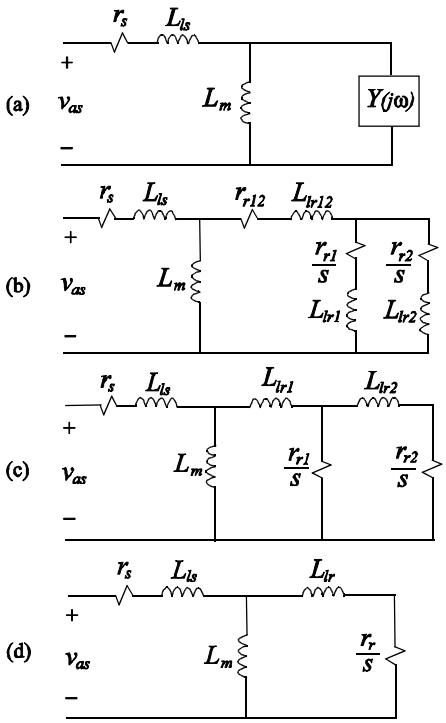

Fig. 1. Induction machine models with different configurations to represent the rotor circuit: (a) Generalized high-order transfer function; (b) and (c) Variations of two branches with resistive and inductive elements to represent the double-cage effect; and (d) Traditional single-rotor-branch configuration.

It is also possible to include the saturation and deep-rotor-bar effect directly into the three phase coupled circuit model as was demonstrated in [3]. However, the increased structural complexity of such models, number of required parameters and test procedures for their determination, etc., may be quite challenging [4]. Although these models provide great accuracy for many cases, they are generally harder to implement as compared to the standard qd models that are even available as built-in library components in many simulation packages.

Several simpler models have been proposed to represent the so-called double-cage rotor circuit in earlier publications, e.g. [5]–[8]. The approach is based on representing the rotor circuit using several resistive and inductive elements that are arranged in two rotor branches. This is schematically depicted in equivalent circuits in Fig.

1(b) and (c). In [7], several dynamic models with similar configurations have been compared. These and similar variations proposed in the literature increase the order of the circuit by one additional branch with the goal of capturing the changes in equivalent rotor resistance, but are still not sufficient for predicting the high-frequency dynamics.

The conventional qd model and its steady state equivalent circuit shown in Fig. 1(d) have the advantage of low-order and simplicity, which explains its wide acceptance and use. Since in general it is not possible to have a model that is accurate in wide range of frequencies without increasing its dynamic order as in [2], we propose to modify the conventional low-order model with a single rotor branch [1] to better predict at least the low-frequency deep-rotor-bar effect during electromechanical transients. The motivation of this approach is to improve the accuracy of traditional model, without adding structural complexity as in [5] – [8], such that it can be readily adopted by many engineers and possibly implemented in commonly-used simulation packages.

2. PROPOSED MODEL

In the following discussion, all rotor parameters are referred to the stator side. As well known, the equivalent rotor resistance, denoted here as r_r, changes with the frequency of rotor currents and slip due to the deep-rotor-bar effect, which depends on the rotor design [8]. During electromechanical transients in wide range of speeds (from stall to nominal), the effective changes in r_r may be quite significant. In general, at very low slip frequency, the equivalent resistance will be smaller and it will increase with the frequency due to the inductance and skin effect in the rotor bars.

For the purpose of discussion in this paper, the values of the rotor resistance at low slip ($s \approx 0$) and at stall ($s \approx 1$) are denoted by r_{r1} and r_{r2}, respectively, as depicted in Fig. 2. The high value of the rotor resistance r_{r2} may be readily estimated by performing the standard blocked-rotor test at which the rotor frequency is 60 Hz.

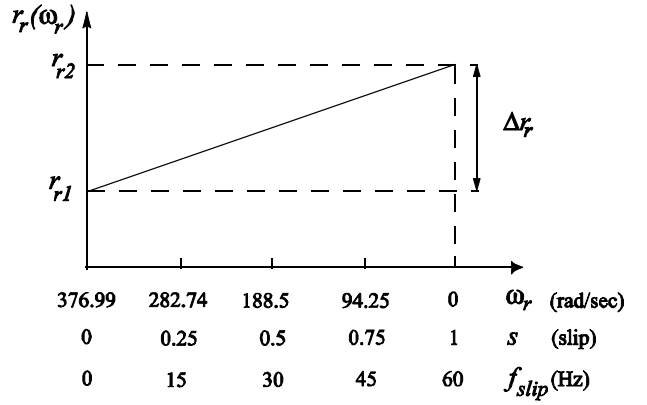

Fig. 2. Approximated speed-dependent equivalent rotor resistance.

At low-slip (close to nominal speed), the equivalent rotor resistance r_{r1} may be calculated using the equivalent circuit Fig. 1(d) and the following approach. The corresponding steady-state torque-speed characteristic is

$$T_e = 3\frac{P}{2}\frac{V_{th}^2}{\omega_e}\cdot\frac{r_r/s}{\left(R_{th}+r_r/s\right)^2+\left(X_{th}+X_r\right)^2}. \quad (1)$$

Here, ω_e is the electrical frequency of the source, and P is the number of poles. The Thevenin equivalent voltage V_{th}, resistance R_{th}, and reactance X_{th} are derived from the equivalent circuit of Fig. 1(d) [8]. At very low slips, the torque may be approximated as

$$T_e \approx 3\frac{P}{2}\frac{V_{th}^2}{\omega_e}\cdot\frac{r_r/s}{\left(r_r/s\right)^2} = 3\frac{P}{2}\frac{V_{th}^2}{\omega_e}\cdot\frac{s}{r_r}. \quad (2)$$

which is linearly proportional with the slip. Based on this approximation, rotor resistance r_{r1} can be estimated by measuring the torque and speed of a slightly loaded motor. Although it is also possible to find the values of the equivalent rotor resistance anywhere in between $s \approx 0$ and $s \approx 1$ by applying different frequency, for the purpose of this paper all intermediate values are obtained using linear interpolation between r_{r1} and r_{r2} as depicted in Fig. 2.

This paper suggests that as long as objectives of the modeling are focused on predicting the low frequency electromechanical transients, the frequency-dependent equivalent rotor resistance r_r depicted in Fig. 2 may be represented as a function of rotor speed ω_r. Based on linear approximation of Fig. 2, this dependency can be compactly expressed in the following form

$$r_r\left(\omega_r\right) = r_{r1} + \Delta r_r \cdot s \quad (3)$$

where $\Delta r_r = r_{r2} - r_{r1}$. This result is then substituted into the standard equivalent circuit of Fig. 1(d) to obtain a modified steady-state equivalent circuit shown in Fig. 3.

To illustrate the effect of such speed-dependent rotor resistance $r_r(\omega_r)$ on the steady-state torque-speed characteristic, we calculated the torque for three models and the resulting curves are shown in Fig. 4. Here, Model 1 and Model 2 are based on standard equivalent circuit of Fig. 1(d) and use fixed rotor resistances. In particular, in Model 1 the rotor resistance has been set to its low-slip value r_{r1}, and in Model 2 the rotor resistance corresponds to the standstill value r_{r2}, respectively.

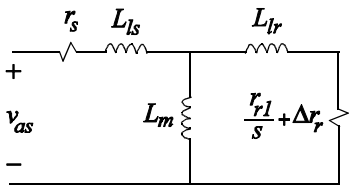

Fig. 3. Modified steady-state equivalent circuit including variation of rotor resistance.

The third Proposed Model corresponds to the modified equivalent circuit depicted in Fig. 3. The characteristics shown in Fig. 4 correspond to the induction machine considered in this paper. An important observation is that the proposed equivalent circuit of Fig. 3 captures both high starting torque (due to increased rotor resistance at stall) and steep torque at nominal speed (due to reduced rotor resistance at low slip), as desired.

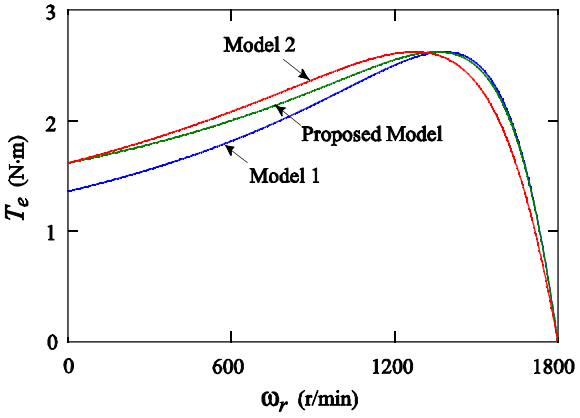

Fig. 4. Steady-state torque-speed characteristic for three models with different rotor resistances.

The results of speed-dependent equivalent rotor resistance demonstrated in steady state in Figs. 2 – 4 can be further applied to a transient model. In this paper we show a very straightforward method of including such speed-dependent rotor resistance in a classical qd model [1]. For consistency, the model equations are included here. In particular, the voltage equations in arbitrary reference frame are

$$v_{qs} = r_s i_{qs} + \omega\lambda_{ds} + p\lambda_{qs} \tag{4}$$

$$v_{ds} = r_s i_{ds} - \omega\lambda_{qs} + p\lambda_{ds} \tag{5}$$

$$v_{qr} = r_r(\omega_r)\, i_{qr} + (\omega - \omega_r)\lambda_{dr} + p\lambda_{qr} \tag{6}$$

$$v_{dr} = r_r(\omega_r)\, i_{dr} - (\omega - \omega_r)\lambda_{qr} + p\lambda_{dr} \tag{7}$$

where ω is the reference frame speed. The corresponding flux linkages are given as

$$\lambda_{qs} = L_{ls} i_{qs} + \lambda_{mq} \tag{8}$$

$$\lambda_{ds} = L_{ls} i_{ds} + \lambda_{md} \tag{9}$$

$$\lambda_{qr} = L_{lr} i_{qr} + \lambda_{mq} \tag{10}$$

$$\lambda_{dr} = L_{lr} i_{dr} + \lambda_{md} \tag{11}$$

$$\lambda_{mq} = L_m\left(i_{qs} + i_{qr}\right) \tag{12}$$

$$\lambda_{md} = L_m\left(i_{ds} + i_{dr}\right) \tag{13}$$

The developed electromagnetic torque is calculated as

$$T_e = \frac{3P}{4}\left(\lambda_{ds} i_{qs} - \lambda_{qs} i_{ds}\right). \tag{14}$$

It should be noted that, by making the rotor resistance speed-dependent, the modified qd model now includes the deep-rotor-bar effect at least in the range of low frequency applicable to electromechanical transients.

3. EXPERIMENTAL VERIFICATION

The induction motor considered in this paper has been characterized using standard no-load and blocked-rotor tests. Several additional measurements in the low-slip region were taken to estimate the equivalent rotor resistance at low frequency based on (2) by loading the motor. The machine parameters are summarized in Appendix.

To compare several models with the actual hardware, we have implemented a startup transient of the motor-dynamometer system available in our lab. The motor was fed from a low-voltage three phase Variac and step-down transformer. A comprehensive custom-built data acquisition system based on NI card interfaced with PC was used to capture and record all three phase currents, voltages, and speed during the acceleration of the motor. For simulation studies, the conventional qd model and the proposed model were implemented in MATLAB-Simulink [9]. To include the effects of non-idealities in the voltage source, i.e. source impedance and harmonics, the actual measured and recorded stator voltages have been imported in the Simulink models to reproduce the same excitation as applied to the hardware and the models. The applied voltage was a bit below the nominal level as to reduce the effect of saturation. Two conventional qd models have been considered. In Model 1 the rotor resistance has been set to its low-slip value r_{r1}, and in Model 2 the rotor resistance has been set to the standstill value r_{r2}, respectively.

The predicted transient responses and the hardware measurements are superimposed in Figs. 5–7. Fig. 5 shows the stator current i_{as} during the initial transient going into a steady state. Fig. 6 shows the same stator current magnified in the middle of transient for clarity. During this time, the motor speed is significantly below its nominal value and the slip is high too. This explains why the Model 1 which uses constant rotor resistance r_{r1} (and Model 2 which uses r_{r2}) overestimates (underestimates) the stator current. As was observed, the proposed model has also a better match with the measurement during both the initial transient and the steady state period. Fig. 7 illustrates the corresponding measured and predicted mechanical speed of the motor. The electromagnetic torque predicted by the three models is shown in Fig. 8. Model 1 with the smallest rotor resistance r_{r1} initially develops slightly less torque, which explains its lower speed in Fig. 7. Model 2 predicts the initial torque better, but results in a lower steady state speed due to higher rotor resistance r_{r2}. However, the proposed model demonstrates the stator currents as well as the speed that are more consistent with the measurements.

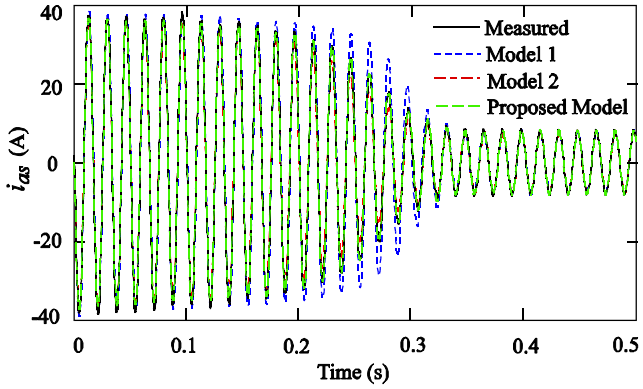

Fig. 5. Stator currents as measured and as predicted by the three models.

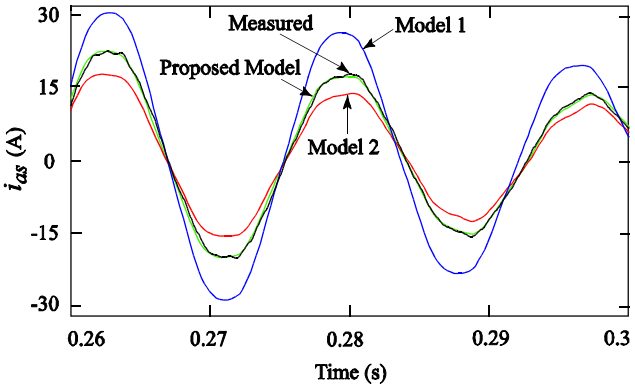

Fig. 6. Magnified stator currents as measured and as predicted by the three models.

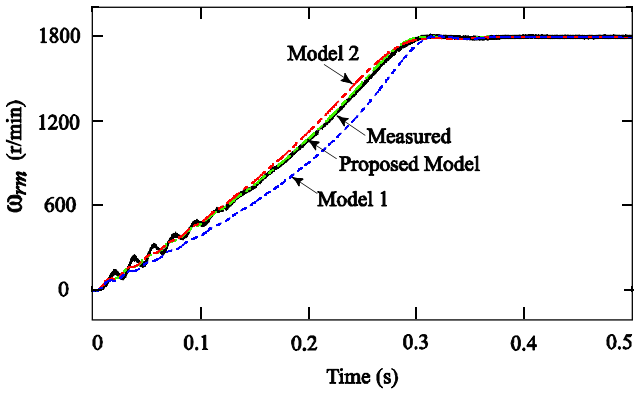

Fig. 7. Rotor speeds as measured and as predicted by the three models.

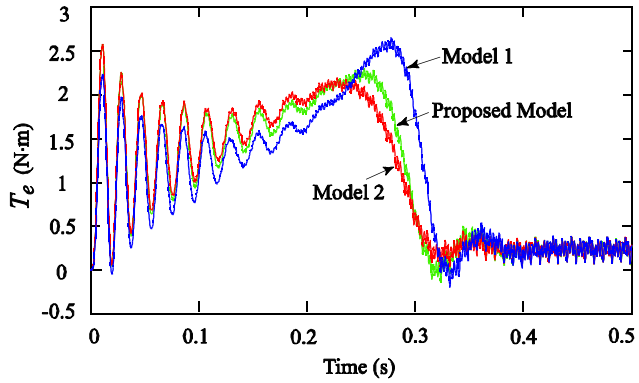

Fig. 8. Electromagnetic torques as predicted by the three models.

4. CONCLUSION

The proposed induction machine model includes the speed-dependent equivalent rotor resistance, which is shown to be adequate for modeling the deep-rotor-bar effect during the low-frequency electromechanical transients. The proposed methodology does not require increasing the order of the model and/or adding branches in the rotor equivalent circuit. The advantageous features include simplicity, ease of implementation, and readily measurable parameters.

5. APPENDIX

Machine parameters: 0.25 hp, 34V, 60 Hz, P=4, 1750 rpm, $r_s = 0.17\Omega$, $X_{ls} = 0.19\Omega$, $X_m = 3.1\Omega$, $r_{r1} = 0.07\Omega$, $r_{r2} = 0.12\Omega$, $X_{lr} = 0.19\Omega$, $J = 0.0023\ \mathrm{kg \cdot m^2}$.

Speed (rpm)	170	450	680	1150	1680
Friction Torque $(N \cdot m)$	0.16	0.19	0.20	0.21	0.22

6. REFERENCES

[1] P. C. Krause, O. Wasynczuk, and S. D. Sudhoff, *Analysis of Electric Machinery and Drive Systems*, 2nd Edition, IEEE Press, Piscataway, NJ, 2002.

[2] S. D. Sudhoff, D. C. Aliprantis, B. T. Kuhn, and P. L. Chapman, "An induction machine model for predicting inverter-machine interaction," *IEEE Trans. on Energy Conversion*, vol. 17, no. 2, pp. 203–210, Jun. 2002.

[3] M. Ikeda, and T. Hiyama, "Simulation studies of the transients of squirrel-cage induction motors," *IEEE Trans. on Energy Conversion*, vol. 22, no. 2, pp. 233–239, Jun. 2007.

[4] S. D. Sudhoff, D. C. Aliprantis, B. T. Kuhn, and P. L. Chapman, "Experimental characterization procedure for use with an advanced induction machine model," *IEEE Trans. on Energy Conversion*, vol. 18, no. 1, pp. 48–56, Mar. 2003.

[5] A. C. Smith, R. C. Healey, and S. Williamson, "A transient induction motor model including saturation and deep-rotor-bar effect," *IEEE Trans. on Energy Conversion,* vol. 11, no. 1, pp. 8–15, Mar. 1996.

[6] J. R. Willis, and B. K. Johnson, "Tailoring induction motor analytical models to fit known motor characteristics and satisfy particular study needs," *IEEE Trans. on Power Systems*, vol. 6, no. 3, pp. 959–965, Aug. 1991.

[7] W. Levy, C. F. Landy and M. D. McCulloch, "Improved models for the simulation of deep bar induction motors," *IEEE Trans. on Energy Conversion*, vol. 5, no. 2, pp. 393–400, Jun. 1990.

[8] P. C. Sen, *Principles of electric machines and power electronics*, 2nd Edition, John Wiley & Sons, 1996.

[9] *Simulink Dynamic System Simulation Software* – Users Manual, MathWorks, Inc., Natick, Massachusetts, 2005.